Comparison of Monte Carlo simulations and nonlocal calculations of the electron distribution function in a positive column plasma

U. Kortshagen,[1,*] G. J. Parker,[2] and J. E. Lawler[1]
[1]*University of Wisconsin–Madison, Department of Physics, 1150 University Avenue, Madison, Wisconsin 53706*
[2]*Lawrence Livermore National Laboratory, P.O. Box 808, L-418 Livermore, California 94550*
(Received 2 April 1996; revised manuscript received 15 July 1996)

Recently the nonlocal approximation for solving the Boltzmann equation to determine the electron distribution function (EDF) in modeling of low-pressure discharges has attracted great interest. The nonlocal approximation is strictly applicable only to electrons which are confined in the plasma volume by the space charge electric field. The unconfined electrons which have a sufficiently high total energy to overcome the space charge potential barrier in front of the walls, and which can therefore be lost from the plasma to the walls, are not consistently addressed by the nonlocal approximation. We compare EDF's from nonlocal calculations in positive column plasmas with and without inclusion of the wall losses in different approximations to results of an efficient, accurate Monte Carlo benchmark method. The expected range of (column radius)×(gas density) for applicability of the nonlocal approach with wall losses is confirmed. The anisotropy of the EDF caused by wall losses of unconfined electrons and by the axial electric field is studied using Monte Carlo simulations. The impact of the anisotropy on the applicability of the nonlocal approximation is discussed. The importance of the appropriate inclusion of the wall losses of unconfined electrons in the nonlocal approximation is demonstrated. An approximation of the treatment of the wall losses in nonlocal calculations is studied, which yields good agreement with the Monte Carlo results in the entire applicable range of the nonlocal approximation. [S1063-651X(96)03512-X]

PACS number(s): 51.10.+y, 52.65.Pp, 52.80.Hc

I. INTRODUCTION

In recent years the modeling of nonequilibrium (glow discharge) plasmas has gained in importance for the development and understanding of plasma sources, e.g., for plasma processing and for lighting applications [1]. One of the major challenges in this area is the development of a simple but realistic description of the spatial dependence of the electron distribution function (EDF) in spatially inhomogeneous nonequilibrium plasmas. These EDF's typically deviate significantly from Maxwell-Boltzmann distributions [2–4]. A number of methods to treat this problem have been developed, and have been successfully applied to a variety of problems, e.g., the Monte Carlo method [5–9], the particle in cell method [10–15], the convected scheme method [16–21], or the direct numerical integration of the electron Boltzmann equation [22–27].

However, the above methods are often rather slow, even using advanced workstations, if spatially multidimensional systems are considered. The growing necessity to develop spatially two- or three-dimensional discharge models has caused a resurgence of interest in semianalytical approximation methods in recent years [25,28–30]. One of these methods which is particularly suited for low-pressure, weakly collisional plasmas is the ''nonlocal approximation,'' which was first proposed by Bernstein and Holstein in 1954 [31]. For higher pressures the ''local approximation'' (sometimes also called ''local-field approximation'') is frequently used (e.g., [32–38]). Usually a more efficient treatment of the problem is achieved by these methods at the expense of a restricted range of applicability and some uncertainty in overall accuracy. Therefore, it is an important and necessary task to test the validity and range of applicability of approximation methods. Such tests have recently been performed in a number of investigations [25,27,26,39]. However, the methods used for comparison in these studies, although more general than the approximate approaches being tested, are themselves frequently subjected to a number of assumptions and restrictions. This is reflected, for instance, in the general disagreement about boundary conditions to be applied in a direct integration of the Boltzmann equation [22–27].

It is desirable to develop benchmark methods for the treatment of the spatially dependent electron kinetics. A benchmark method should rely only on a minimum number of restrictive assumptions and/or mathematical approximations, and it should provide no ambiguity in the specification of boundary conditions. Monte Carlo methods are in many respects the best suited to serve as benchmark methods. Errors in the Monte Carlo simulations are well understood, because they are essentially just statistical (assuming a particular set of cross sections and boundary conditions). A Monte Carlo approach can be formulated from first principals without imposing velocity space boundary conditions on the EDF. Furthermore, in cases where the particle motion can be described analytically, the errors caused by numerical inaccuracies can be greatly reduced. Although Monte Carlo codes are often not fast enough to be run self-consistently with Poisson's equation, they can still be used to test other approximations by importing the electric potential distribution.

*Permanent address: University of Minnesota–Twin Cities, Department of Mechanical Engineering, 111 Church Street S.E., Minneapolis, MN 55455.

In this paper we present a highly realistic five-dimensional (two spatial and three velocity dimensions) Monte Carlo code. We apply this code to a dc positive column plasma, which has recently attracted renewed attention as a model system for the study of the space dependence of the electron kinetics in nonequilibrium plasmas [24,21,25–27].

We use our Monte Carlo code as a benchmark method for testing over a range of parameter space a code based on the ''nonlocal approximation.'' The nonlocal code finds a solution of a spatially averaged kinetic equation, and reduces the space-dependent description of the electron kinetics to an effectively one-dimensional problem. The space dependence of the EDF is derived from a ''generalized Boltzmann relation'' in the nonlocal method. The general validity of this approach for weakly collisional plasmas has been demonstrated in a number of experimental [40–42,29] as well as theoretical investigations [25,27,39]. However, the ''nonlocal approach'' applies strictly only to the confined electrons, i.e., those electrons which have a total energy too low to overcome the space charge potential in order to escape to the discharge walls. The ''unconfined'' electrons, which possess a high enough energy to reach the walls, are not modeled in a completely satisfactory fashion. This problem has been discussed [30], but has not been thoroughly investigated in the literature. The importance of the unconfined electrons is obvious from the fact that in a steady-state diffusion-dominated discharge the rate of loss of electrons to the wall exactly matches the rate of ionization. An inaccurate treatment of the wall losses of unconfined electrons will thus immediately result in an erroneous ionization balance. The wall loss rate also determines the value of the wall potential relative to the plasma, which is important for many applications. Furthermore, the wall losses may enhance the anisotropy of the EDF. We are not aware of any thorough explorations of this effect, and whether it limits the applicability of the nonlocal approximation, which relies on a moderate anisotropy of the EDF. The Monte Carlo method allows a rigorous study of this problem without the necessity of using approximate boundary conditions in velocity space.

The paper is organized as follows: In Sec. II we explain the physical assumptions used in our discharge models. Details on the Monte Carlo method are presented in Sec. III. The ''nonlocal'' discharge model is briefly described in Sec. IV. A study of the anisotropy of the EDF caused by both the wall losses of the electrons and by the axial electric field, and an investigation of the applicable range of the nonlocal approximation using a particular treatment of the unconfined electrons is given in Sec. V. In Sec. VI the conclusions are summarized and some planned future work is outlined.

II. PHYSICAL ASSUMPTIONS OF THE DISCHARGE MODELS

The classic positive column discharge is emphasized in this study. Positive columns have been studied intensively since the seminal works by Schottky [43] and Tonks and Langmuir [44]. Schottky modeled a relatively high-pressure positive column in which ion motion is limited by collisions with the background gas (mobility limited), and ion transport is well described by the concept of ambipolar diffusion. Tonks and Langmuir modeled a relatively low-pressure positive column in which ion motion is limited by inertia and ion transport is well described by the free-fall model. Both works incorporated the assumption of a Maxwellian electron distribution. In more recent decades the study of ''diffusive cooling'' of electrons in positive columns has been pursued [45,46,24,21]. Diffusive cooling refers to precisely the kind of effect we are studying in this work. Although much is understood about positive columns, scientific interest has remained high because of the very widespread use of positive column discharges as sources of incoherent and coherent light.

Only single-step ionization is included in the models used in this work. We are primarily interested in the effect of the radial (space charge) fields on the electron distribution function. Any comparison of such model results to experimental results should be limited to lower radius$\times$gas density products, $R\times N$, where single-step ionization is dominant.

Elastic scattering in the models uses the ''momentum transfer'' approximation in which electrons are redistributed isotropically after a scattering event. The elastic momentum transfer cross section is [32].

$$\sigma_{\mathrm{el}}=\begin{cases} 1.59\times10^{-15}\ \mathrm{cm}^2\times u/u_{\mathrm{ex}} & \text{for } u<u_{\mathrm{ex}} \\ 1.59\times10^{-15}\ \mathrm{cm}^2\times\sqrt{u_{\mathrm{ex}}/u} & \text{for } u>u_{\mathrm{ex}}, \end{cases} \tag{1}$$

where u is the electron kinetic energy, and $u_{\mathrm{ex}}=11.55\mathrm{eV}$ is the excitation threshold energy. An elastic recoil energy loss on average of 2.73×10^{-5} of the incident kinetic energy is used in all simulations. We are modeling an ''argonlike'' gas. Only one inelastic scattering process is included in the model. The cross section for this inelastic scattering process is

$$\sigma_{\mathrm{ex}}=1.56\times10^{-16}\ \mathrm{cm}^2\times\ln(u/u_{\mathrm{ex}})/(u/u_{\mathrm{ex}}) \tag{2}$$

for electrons with $u>u_{\mathrm{ex}}$, and zero otherwise. Inelastically scattered electrons lose 11.55 eV, and are also redistributed isotropically. The single-step ionization cross section is

$$\sigma_i=3.18\times10^{-16}\ \mathrm{cm}^2\times\ln(u/u_i)/(u/u_i) \tag{3}$$

for electrons with $u>u_i=15.9$ eV, and zero otherwise. Both the ejected and scattered electrons are redistributed isotropically, and both electrons equally share the available energy (kinetic energy of the incident electron less threshold energy of $u_i=15.9$ eV). The isotropic scattering approximation for inelastic and ionizing collisions is often used in positive column models. It is a physically reasonable approximation because the electrons involved in such processes in a positive column are mainly just above threshold.

It is often assumed in positive column models that all electrons reaching the column wall recombine with an ion. This assumption will be used in our models.

A range of radius$\times$gas density products, $R\times N$, is explored in this study. The range extends from 1×10^{14} to $3\times10^{16}\ \mathrm{cm}^{-2}$, with the radius R fixed at 1.0 cm. The nonlocal approximation is expected to work very well at the lower end of the range, at least for the confined electrons.

The radial potential energy for electrons will be approximated as harmonic $(-e\Phi(r)=b_1r^2)$ from the axis to within

one radial cell of the column wall ($\frac{1}{25}$ of the radius). Here r is the radius in cylindrical coordinates, $\Phi(r)$ is the electrostatic potential, and b_1 is a constant. The potential energy is continuous at the inner boundary of the last cell, harmonic $(-e\Phi(r)=a_2+b_2r^2)$ in the last cell, and continuous to the wall potential energy $-e\Phi_w$. These approximations result in a discontinuity in the slope of the radial potential (radial field) at the inner boundary of the last cell. The harmonic potential approximation is arguably correct near the axis of the column from symmetry considerations. The harmonic potential approximation greatly accelerates the Monte Carlo simulations. In later investigations, this approximation will be avoided. The radial potential energy $-e\Phi_{\rm sh}$ at the inner boundary of the outermost radial cell is assumed to be 8 eV above the axial potential energy. A steep change in potential $(\Phi_w-\Phi_{\rm sh})$ in the outermost cell represents the plasma sheath.

The axial electric field E_z and the potential drop $\Phi_w-\Phi_{\rm sh}$ of the sheath in the outermost radial cell are both found self-consistently using two constraints. The first constraint is that wall losses of electrons be balanced by ionization. The second constraint is that the average ionization rate per unit volume matches the average ion loss rate per unit volume from the ambipolar diffusion equation,

$$\frac{D_s}{\Lambda^2}\overline{n}=\overline{n\nu_i}. \tag{4}$$

Here $\overline{n\nu_i}$ is the average ionization rate per unit volume, $\Lambda=R/2.405$ is the typical diffusion length, and $\overline{n}$ is the average electron density. For the ambipolar diffusion coefficient D_s we use an approximation proposed by Ingold [47], which approaches the free-fall Tonks-Langmuir case in the small $R\times N$ limit as well as the collision-dominated Schottky case in the large $R\times N$ limit: $D_s=D_a/(1+2\overline{n\nu_i}/(\overline{n\nu_{cx}}))$. Here $D_a\approx kT_e\mu_i/e$ is the usual ambipolar diffusion coefficient from the Schottky theory, where k is the Boltzmann constant, $\mu_i=e/M_i\nu_{cx}$ is the ion mobility, and $\nu_{cx}=Nv_iQ_{cx}$ is the ion-neutral charge exchange collision frequency where N is the neutral gas density, v_i the thermal speed of the ions, and $Q_{cx}=40\times10^{-20}$ m^2 the charge exchange cross section. M_i is the (argon) ion mass. The electron temperature T_e is approximated as $\frac{2}{3}$ of the mean kinetic energy of the EDF in the discharge center divided by the Boltzmann constant k. Both constraints are fulfilled with an accuracy of better than 2% at the lower three gas densities, and within 5% for the higher three gas densities.

III. DETAILS OF THE MONTE CARLO CODE

Some of the details of the Monte Carlo code used to simulate electron kinetics and transport in the positive column are outlined in this section. The code uses a null collision approach based on von Neumann's method of rejection to eliminate any numerical integration [48]. The use of a piecewise harmonic radial potential is a key approximation because it makes the ballistic radial motion completely analytic.

It is both convenient and physically reasonable to choose a model set of cross sections such that the collision rate, $N\sigma_tv$, has an absolute maximum for any electron energy. Here σ_t is the total cross section (note: $\sigma_t=\sigma_{\rm el}+\sigma_{\rm ex}+\sigma_{\rm ion}$), and v is the electron speed. In a Monte Carlo simulation based on mean free times the differential probability dP of a collision in the distance increment ds along an electron trajectory is

$$dP=\exp\left(-\int_0^s\sigma_tNds\right)\sigma_tNds. \tag{5}$$

The cumulative probability $P(s)$ of a collision within a distance s along the electron's trajectory is

$$P(s)=1-\exp\left(-\int_0^s\sigma_tNds\right). \tag{6}$$

This cumulative probability is set equal to a pseudo-random-number r_1 on the (0, 1) interval

$$r_1=P(s_c) \tag{7}$$

to define the distance, s_c, where the next collisions occurs along the trajectory.

The equation

$$\ln(1-r_1)=\int_0^{s_c}\sigma_tNds=N\int_0^{t_c}\sigma_tv\,dt \tag{8}$$

must be solved in order to find s_c or the elapsed time, t_c, until the next collision. The integral becomes analytic by adding the fictitious null cross section σ_n, which makes the integrand constant by making $(\sigma_t+\sigma_n)v$ independent of the electron kinetic energy and equal to the maximum of σ_tv [49,50,5]. Thus we find

$$t_c=\frac{\ln(1-r_1)}{N(\sigma_tv)_{\max}}. \tag{9}$$

Five variables are needed because two spatial and three velocity coordinates are tracked. We find a convenient set of variables to be: the axial or z component of the speed, v_z, where the z axis is the column axis; the total (potential plus kinetic) z energy, ε_z; the radius squared, r^2, in a cylindrical coordinate system; the radial velocity, v_r; and the total (potential plus kinetic) energy in the plane perpendicular to the z axis, $\varepsilon_{\rm perp}$. During ballistic motion, two of the coordinates are constant, and three need to be updated. Clearly v_z at the next collision is

$$v_{zc}=v_{z0}-\frac{eE_z}{m}t_c, \tag{10}$$

where v_{z0} is the coordinate value at the preceding collision, and where E_z is the axial electric field, $-e$ the electron charge, and m the electron mass. The first integral of the equation of motion in the perpendicular plane is

$$\frac{m}{2}v_r^2+\frac{L_z^2}{2mr^2}+a_j+b_jr^2=\varepsilon_{\rm perp}, \tag{11}$$

where L_z is the angular momentum about the column or z axis, and a_j and b_j define the harmonic potential in the jth radial cell. A convenient change of variable is to define

$$\beta = r^2 + \frac{(a_j - \varepsilon_{\rm perp})}{2b_j}. \tag{12}$$

The first integral of the harmonic oscillator equation is recovered as

$$(\dot{\beta})^2 + \frac{8b_j}{m}\beta^2 = \frac{8b_j}{m}\left(\frac{a_j - \varepsilon_{\rm perp}}{2b_j}\right)^2 - \frac{4L_z^2}{m^2}. \tag{13}$$

The analytic solution used to advance r^2 and v_r is

$$\beta(t) = \sqrt{\beta_0^2 + (\dot{\beta}_0/\omega)^2} \times \cos(\omega t + \Theta), \tag{14}$$

$$\dot{\beta}(t) = 2rv_r = -\omega\sqrt{\beta_0^2 + (\dot{\beta}_0/\omega)^2} \times \sin(\omega t + \Theta), \tag{15}$$

where

$$\omega = \sqrt{8b_j/m} \tag{16}$$

and

$$\Theta = -\tan^{-1}\left(\frac{\dot{\beta}_0}{\omega\beta_0}\right). \tag{17}$$

This analytic solution is conveniently structured to evaluate the minimum time t_b required for the electron to penetrate a boundary of its current spatial cell. The electron distribution function is sampled at 25 radial cell boundaries, uniformly spaced in r, and is also sampled at 15 axial cell boundaries, uniformly spaced in z. The tracking of the axial motion is maintained in order to eliminate end effects near the cathode and anode in these simulations. These end or sheath effects will be studied in future work. The approach for sampling the distribution function is outlined in [5]. If $t_b < t_c$, then the electron's velocity and energy are evaluated at the cell boundary and contribute to the electron distribution function at the cell boundary. The electron is subsequently released in a different spatial cell with a time $(t_c - t_b)$ remaining until the next collision. When the electron penetrates a spatial cell wall all of its coordinates change continuously, but there is a possibility of a discontinuity in the radial electric field. The potential defined by a_j and b_j is continuous, but can have discontinuities in its slope at radial cell boundaries. In future work we will explore how fine a radial mesh is required in order to eliminate errors from a discontinuous radial field. It seems extremely likely that a mesh cell size comparable to the electron mean free path would eliminate errors, but it may not be necessary to use such small cells.

In these comparisons to the nonlocal model we assume that a_j and b_j are the same in all but the outermost radial cell. The only discontinuity in the radial field therefore occurs at the radial sheath boundary.

Once an electron has been advanced to the location of a collision, the procedure described by Boeuf and Marode is used to determine the type of collision [5]. If a null collision occurs the electron is released with no changes in any of its coordinates. Excitation and ionization events are tracked in each spatial cell. The location and kinetic energy of each secondary electron is stored, and its motion is subsequently followed. Electrons leave the simulation when they reach the absorbing outer radial wall or the anode at the end of the column. A positive column simulation should have wall losses matched by ionization in each axial cell. Too large (or too small) an axial field for a given radial potential causes the electron current to grow (or shrink) exponentially along the z axis.

We actually developed several versions of this code in order to test the versions against each other, and eliminate any possible coding errors. Versions were written in FORTRAN, C, and FORTH. All ran well on desktop computers with an Intel 486 or faster processor. Usually 10^6 electrons are followed. The calculation times are of the order of several hours to days for the self-consistent calculations.

IV. NONLOCAL MODEL

The nonlocal approximation has recently attracted great attention, and it has been discussed in detail in a number of review articles. Thus only a brief description of the method is presented here. For more details the reader is referred to Refs. [51,52,27]. The problem of the electron losses to the walls is treated in more detail here.

In a typical dc positive column the average energy gain of electrons between two collisions is usually small compared to their average kinetic energy, and elastic collisions are much more likely than inelastic collisions, so that the EDF is usually approximated by the well-known two-term expansion into spherical harmonics [53,54]. Since the EDF lacks any axial and azimuthal dependence, it is represented as $\mathcal{F}(r,\mathbf{v}) = \mathcal{F}_0(r,v) + \mathbf{v}/v \cdot \boldsymbol{\mathcal{F}}_1(r,v)$, with the normalization $\int \mathcal{F}(r,\mathbf{v}) d^3v = n(r)$, and with n the electron density.

The nonlocal approximation addresses weakly collisional plasmas, where the energy relaxation length

$$\lambda_\epsilon(u) = \sqrt{\lambda_m(u)\lambda^*(u)} \tag{18}$$

exceeds the discharge dimensions in the range of kinetic energies of interest [55], where $\lambda_m(u) = (N\sigma_{\rm et}(u))^{-1}$ is the mean free path length for elastic momentum transfer of the electrons, and $\lambda^*(u) = [N(\sigma_{\rm ex}(u) + \sigma_i(u))]^{-1}$ is the mean free path length for all kinds of inelastic collision processes. In this case a typical electron moves across the discharge without a significant change of its total energy (i.e., the sum of kinetic plus potential energy). It is therefore assumed that the isotropic part of the EDF, $\mathcal{F}_0(r,v)$, when represented as a function of total energy

$$\varepsilon = u - e\Phi(r) = \frac{mv^2}{2} - e\Phi(r) = \frac{mv_z^2}{2} + \varepsilon_{\rm perp}, \tag{19}$$

is essentially spatially constant [31,55]:

$$\mathcal{F}_0(r,v) \rightarrow F_0(r,\varepsilon) = F_0^{(0)}(\varepsilon) + F_0^{(1)}(r,\varepsilon). \tag{20}$$

The validity of the nonlocal approximation requires that $F_0^{(0)}(\varepsilon) \gg |F_0^{(1)}(\varepsilon,r)|$. The spatially constant main part of the EDF, $F_0^{(0)}$, is calculated from a spatially averaged kinetic equation, which is an ordinary differential equation in total energy [55]:

$$\frac{d}{d\varepsilon}\left(\overline{u^{1/2}D_\varepsilon}\frac{dF_0^{(0)}(\varepsilon)}{d\varepsilon}+\overline{V_\varepsilon}F_0^{(0)}(\varepsilon)\right)$$
$$=(\overline{u^{1/2}\nu_{\rm ex}}(\varepsilon)F_0^{(0)}(\varepsilon)-\overline{u^{1/2}\nu_{\rm ex}}(\varepsilon+u_{\rm ex})F_0^{(0)}(\varepsilon+u_{\rm ex}))$$
$$+(\overline{u^{1/2}\nu_i}(\varepsilon)F_0^{(0)}(\varepsilon)-\overline{I^+}(\varepsilon))+\overline{u^{1/2}\nu_w}(\varepsilon)F_0^{(0)}(\varepsilon). \quad (21)$$

Here ν_w denotes an effective wall loss frequency which is discussed in detail below. The barred quantities denote spatial averages performed over the part of the discharge cross section, which is accessible for electrons with a given total energy:

$$\overline{u^{1/2}D_\varepsilon}=\frac{2e^2E_z^2}{3m}\frac{2}{R^2}\int_0^{r^*(\varepsilon)}\frac{u^{3/2}(r)}{\nu_t(u(r))}rdr, \quad (22)$$

$$\overline{V_\varepsilon}=\frac{2m}{M_a}\frac{2}{R^2}\int_0^{r^*(\varepsilon)}\nu_m(u)u^{3/2}(r)rdr, \quad (23)$$

$$\overline{u^{1/2}\nu_{{\rm ex},i}}(\varepsilon)=\frac{2}{R^2}\int_0^{r^{{\rm ex},i}}\nu_{{\rm ex},i}(u)u(r)^{1/2}rdr, \quad (24)$$

$$\overline{I^+}(\varepsilon)=4\overline{u^{1/2}\nu_i}(2\varepsilon+u_i)F_0^{(0)}(2\varepsilon+u_i). \quad (25)$$

Here $I^+(\varepsilon)$ represents the scattered and secondary electrons which are produced in an ionization event, $\nu_t(u)=N\sigma_t(u)\sqrt{2u/m}$ is the total collision frequency, $\nu_m(u)=N\sigma_{\rm el}(u)\sqrt{2u/m}$ denotes the elastic momentum transfer collision frequency, $\nu_{\rm ex}=N\sigma_{\rm ex}(u)\sqrt{2u/m}$ is the excitation collision frequency with the threshold energy $u_{\rm ex}$, and $\nu_i=N\sigma_i(u)\sqrt{2u/m}$ denotes the ionization frequency with the threshold u_i. The turning point $r^*(\varepsilon)$ of the electron motion is defined by $u(r^*(\varepsilon))=0$. Analogously, the maximal radii $r^{\rm ex}(\varepsilon)$ and $r^i(\varepsilon)$, at which excitation and ionization, respectively, are possible, are defined by $u(r^{{\rm ex},i}(\varepsilon))=u_{{\rm ex},i}$. (See Refs. [51,52,27] for details.)

The spatially dependent EDF of the kinetic energy, $F_0(r,u)$, can be calculated from the EDF of the total energy $F_0^{(0)}(\varepsilon)$ using a ''generalized Boltzmann relation''

$$F_0(r,u)=F_0^{(0)}(\varepsilon=u-e\Phi(r)). \quad (26)$$

In the total energy picture, all electrons which have gained a total energy higher than the potential energy at the wall, $-e\Phi_w$, are able to escape to the wall. For the unconfined electrons with $\varepsilon>-e\Phi_w$, the nonlocal approach does not strictly apply [56], since the assumption that the electrons are reflected by the space charge potential at their turning point is an important prerequisite for the averaging procedure which leads to Eq. (21). However, electrons with a total energy only slightly exceeding the potential energy at the wall (and which are at a distance $\lesssim\lambda_m$ from it) have to move almost normally toward the wall in order to overcome the potential barrier in front of the wall. This means that the velocity vector of the escaping electrons has to be within a loss cone [56]. In planar geometry the derivation of the solid angle $\delta\Omega$ of the loss cone with the aperture angle α_p is straightforward, yielding

$$\delta\Omega(\varepsilon,r)=2\pi[1-\cos(\alpha_p(\varepsilon,r))]$$
$$=2\pi\left[1-\sqrt{\left(\frac{e(-\Phi_w+\Phi(r))}{\varepsilon+e\Phi(r)}\right)}\right]. \quad (27)$$

It was pointed out in Ref. [56] that a rigorous description of the unconfined electrons requires the solution of the space-dependent, nonaveraged kinetic equation

$$\frac{1}{r}\frac{\partial}{\partial r}\left(u^{1/2}D_e r\frac{\partial F_0(r,\varepsilon)}{\partial r}\right)$$
$$+\frac{\partial}{\partial\varepsilon}\left(u^{1/2}D_\varepsilon\frac{\partial F_0(r,\varepsilon)}{\partial\varepsilon}+V_\varepsilon F_0(r,\varepsilon)\right)$$
$$=(u^{1/2}\nu_{\rm ex}(r,\varepsilon)F_0(r,\varepsilon)$$
$$-u^{1/2}\nu_{\rm ex}(r,\varepsilon+u_{\rm ex})F_0(r,\varepsilon+u_{\rm ex}))$$
$$+(u^{1/2}\nu_i(r,\varepsilon)F_0(r,\varepsilon)-I^+(r,\varepsilon)), \quad (28)$$

with $D_e=\lambda_m^2(u)\nu_m(u)/3$ the electron diffusion coefficient, and all other symbols as defined in Eqs. (22)–(25) without performing the spatial averaging. This equation has to be solved subject to the boundary condition that the fraction of the thermal flux of the electrons which is scattered into the loss cone and escapes to the wall is balanced by the diffusion flux from the plasma [55,25]. This boundary condition has to be applied at the sheath boundary $r\approx R$:

$$vF_0\left.\frac{\delta\Omega}{4\pi}\right|_{r\approx R}=-D_e\left.\frac{\partial F_0}{\partial r}\right|_{r\approx R}. \quad (29)$$

Here it should be noted that a zero boundary condition for the EDF was used in Ref. [56] in order to obtain a simple analytical solution of the problem. However, as will become evident below in the discussion of our Monte Carlo results, this boundary condition may overemphasize the spatial dependence of the EDF for $\varepsilon>-e\Phi_w$, at least within the validity range of the nonlocal approximation. In reality, particularly if the loss cone solid angle $\delta\Omega$ is small compared to 4π, only a small fraction of the electrons is actually able to escape to the wall, and the EDF may show only a weak radial dependence.

In order to avoid the complicated procedure of solving Eq. (28) we will rely on the approximate spatial constancy of $F_0(r,\varepsilon)$, and adopt the more approximate procedure of introducing a wall loss term $\overline{u^{1/2}\nu_w}$ into the space-averaged kinetic equation (21), which treats the wall losses essentially as an additional inelastic loss process depleting energetic electrons. The validity of this approach will be discussed below in the comparison to our Monte Carlo results.

In the following we will estimate the wall escape frequency ν_w for electrons in a positive column. It will be assumed that the potential drop between the plasma and the wall is concentrated in the sheath, so that $u(r)\approx u(r=0)=\varepsilon$ for the entire discharge cross section. Instead of solving the stationary diffusion problem Eq. (28) with its source terms (i.e., the electron heating term) and its sink terms (the wall losses and inelastic collisions) we consider the (auxiliary) problem of finding the decay time of the EDF in the energy range $\varepsilon>-e\Phi_w$ which can be identified

with the typical lifetime or wall escape time τ of an electron in the discharge. (This procedure is commonly used in diffusion problems.) Assuming that for electrons in this total energy range the wall losses are much more important than inelastic collisions, we retain only the spatial diffusion term in the kinetic equation for $F_0(r,\varepsilon,t)$ which describes the temporal decay of the EDF:

$$-\frac{\partial F_0(r,\varepsilon,t)}{\partial t}=D_e\frac{1}{r}\frac{\partial}{\partial r}r\frac{\partial F_0(r,\varepsilon,t)}{\partial r}. \tag{30}$$

This equation is solved subject to the boundary condition (29). It has the following fundamental solution:

$$F_0(r,\varepsilon,t)\propto e^{-t/\tau}J_0\left(\frac{r}{\sqrt{D_e\tau}}\right). \tag{31}$$

Here J_0 is the zeroth order Bessel function of the first kind. Inserting Eq. (31) into Eq. (29) yields

$$\frac{J_1(R/\sqrt{D_e\tau})}{J_0(R/\sqrt{D_e\tau})}=\frac{3\sqrt{D_e\tau}}{\lambda_m}\frac{\delta\Omega}{4\pi}, \tag{32}$$

with J_1 is the first-order Bessel function of the first kind. For $\lambda_m \ll R$ the right hand side of Eq. (32) is large compared to unity, and $J_0(R/\sqrt{D_e\tau})$ approaches zero. This yields the well-known lifetime in the diffusion dominated case $\tau_{\rm diff}$:

$$\tau=\tau_{\rm diff}=\left(\frac{R}{2.4}\right)^2\frac{1}{D_e}. \tag{33}$$

In the opposite case the left hand side of Eq. (32) can be expanded into the lowest order, which yields the lifetime in the free flight case $\tau_{\rm ff}$:

$$\tau=\tau_{\rm ff}=0.5\frac{R}{\lambda_m}\frac{4\pi}{\delta\Omega}\frac{1}{\nu_m}. \tag{34}$$

An interpolation for the intermediate regime can be obtained by adding both times: $\tau=\tau_{\rm diff}+\tau_{\rm ff}$. In the free flight case the electron escape time becomes so small that the time which an electron needs to be scattered into the loss cone must be included. This time $\tau_{\rm sc}$ is given by

$$\tau_{\rm sc}=\left(2\nu_m\frac{\delta\Omega}{4\pi}\right)^{-1}. \tag{35}$$

The factor 2 on the right hand side of Eq. (35) arises from the fact that in the free flight case two loss cones have to be considered, as will be illustrated below.

A general interpolation for the wall escape time of the electrons is thus given by

$$\tau=\tau_{\rm diff}+\tau_{\rm ff}+\tau_{\rm sc}=\left(\frac{R}{2.4}\right)^2\frac{1}{D_e}+\frac{1}{2}\left(\frac{R+\lambda_m}{\lambda_m}\right)\frac{4\pi}{\delta\Omega}\frac{1}{\nu_m}. \tag{36}$$

It should be noticed that $\tau_{\rm ff}$ contributes only in the case $\lambda_m \approx R$. In the free flight case $\lambda_m \gg R$ and $\tau \approx \tau_{\rm sc} \gg \tau_{\rm ff}$ and $\tau_{\rm diff}$, and in the highly collisional case $\tau \approx \tau_{\rm diff} \gg \tau_{\rm ff}$ and $\tau_{\rm sc}$.

The expression for the wall escape term in the kinetic equation (21) is given by

$$\overline{u^{1/2}\nu_w}(\varepsilon)\approx\frac{\varepsilon^{1/2}}{\tau}. \tag{37}$$

It should be mentioned that the loss cone approximation of Eq. (27) is actually correct only for an electron in front of a plane wall. This should be a good approximation for electrons in close vicinity to the positive column wall. In the free flight case, however, electrons from the central regions of the discharge also contribute to the wall loss. A more rigorous analysis requires a consideration of the angular momentum. Due to its conservation the loss cone becomes asymmetric except for electrons very close to the wall. In the cylindrical system an electron may reach the wall when its total energy of the perpendicular motion $\varepsilon_{\rm perp}$ surpasses the sum of its potential energy and its centrifugal energy at the wall, i.e., if

$$\varepsilon_{\rm perp}\geqslant -e\Phi_w+\frac{L_z^2}{2mR^2}. \tag{38}$$

For an electron at a radius r, this means

$$\frac{mv_r^2}{2}+\frac{L_z^2}{2mr^2}\geqslant -e(\Phi_w-\Phi(r))+\frac{L_z^2}{2mR^2}. \tag{39}$$

By introducing the angle α as the polar angle of the electron velocity vector referenced to the local radius vector, the radial kinetic energy $mv_r^2/2$ can be expressed as $(\cos^2\alpha)\times u=(\cos^2\alpha)\times(\varepsilon+e\Phi(r))$. One obtains

$$\cos^2\alpha(\varepsilon,r,L_z)\geqslant\frac{-e(\Phi_w-\Phi(r))+\frac{L_z^2}{2m}\left(\frac{1}{R^2}-\frac{1}{r^2}\right)}{\varepsilon+e\Phi(r)}. \tag{40}$$

If the electron has no angular momentum about the z axis , $L_z=0$, then α corresponds to the aperture angle in planar geometry, α_p, as described by Eq. (27). If $L_z\neq 0$, i.e., for finite azimuthal velocity, then the second term in the numerator causes α to increase. The loss cone therefore becomes elliptic, i.e., for the same total energy ε the aperture angle α is smaller for electrons moving in a plane containing the z axis than for electrons moving in the azimuthal plane. As can be seen from Eq. (40) the rotational asymmetry of the loss cone becomes maximal as r tends toward 0, and it disappears if r approaches R. The curved wall appears planar for the electrons very close to it. For electrons close to the axis it may even happen that the forward and backward loss cones (referenced to the closest wall) merge in the azimuthal direction, and form a ''loss band'' in velocity space, as will be demonstrated below. Equation (40) could in principle be used to determine a wall loss rate in a calculation based on a nonlocal model, but the complexity of using Eq. (40) would violate the spirit of the simple nonlocal approach. Therefore we will use the loss cone expression Eq. (27) in the following comparisons to the Monte Carlo results, since, due to the cylindrical geometry even in the free flight case, the major part of the wall escape is carried by electrons close to the wall, for which the loss cone is almost symmetric.

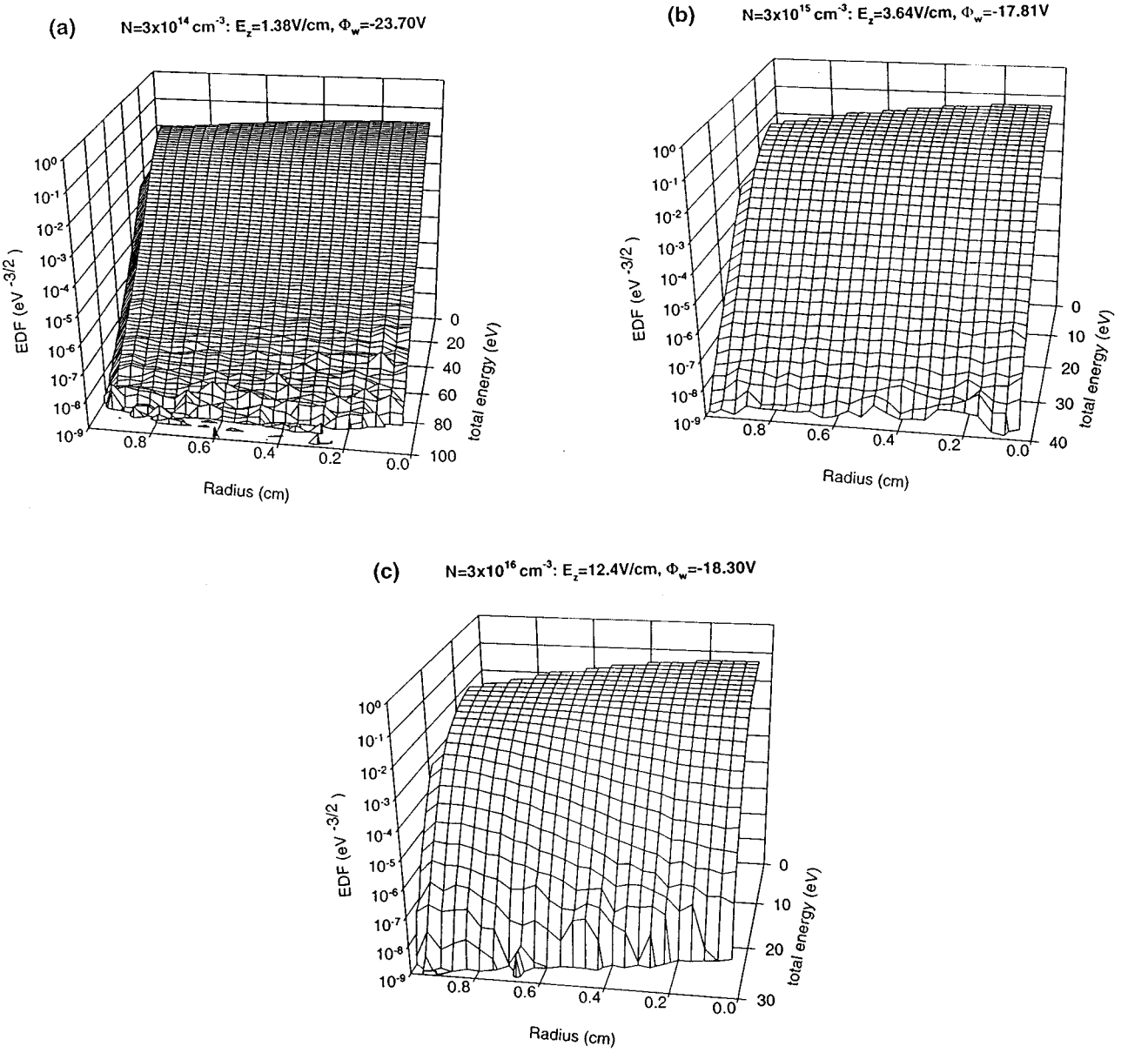

FIG. 1. EDF's from the Monte Carlo calculations plotted as function of the total energy ε and the radius for various pressures. The EDF's are normalized to the electron density at $r=0.04$ cm.

In order to illustrate the effect of the second loss cone in the free flight case, we will also perform nonlocal calculations using only one loss cone, which may be more justified for $\lambda_m \leq R$. This means we neglect the factor of 2 in Eq. (35).

V. RESULTS AND DISCUSSION

In this section we first present and discuss Monte Carlo results which demonstrate that the nonlocal approach is qualitatively correct using the energy and radial dependences of the EDF's. Then we explore angle-resolved EDF's from the Monte Carlo simulations to test the two-term spherical harmonics expansion underlying the nonlocal approach. Here we are concerned about the anisotropy of EDF's in velocity space from the axial field at low N (high E_z/N) and from wall losses at all N. Finally we compare the Monte Carlo results and the results of the nonlocal discharge models with and without wall losses. The inclusion of only single-step ionization in our models means that the absolute electron density is arbitrary. The reader may consider all EDF's presented in the subsequent figures to have been divided by the axial electron density. For example, in comparison to the nonlocal results, we plot $F_0^{(0)}(\varepsilon)/n(r=0)$.

In Fig. 1, EDF's for various neutral gas densities are plotted as a function of the total energy and the radius. At the lower N in Figs. 1(a) and 1(b) the EDF's show a nonlocal behavior, i.e., they are spatially constant for a given total energy. Only at the wall do the EDF's drop due to the wall loss of electrons. At the highest pressure in Fig. 1(c) the EDF also shows deviations from the nonlocal behavior in the plasma bulk. For a given total energy the EDF decreases toward the discharge axis. The reason for this decrease has been discussed in detail elsewhere. It is basically due to the effect that for a given total energy the kinetic energy of the electrons is maximum in the discharge center, and therefore so is the efficiency of the inelastic collisions which lead to a

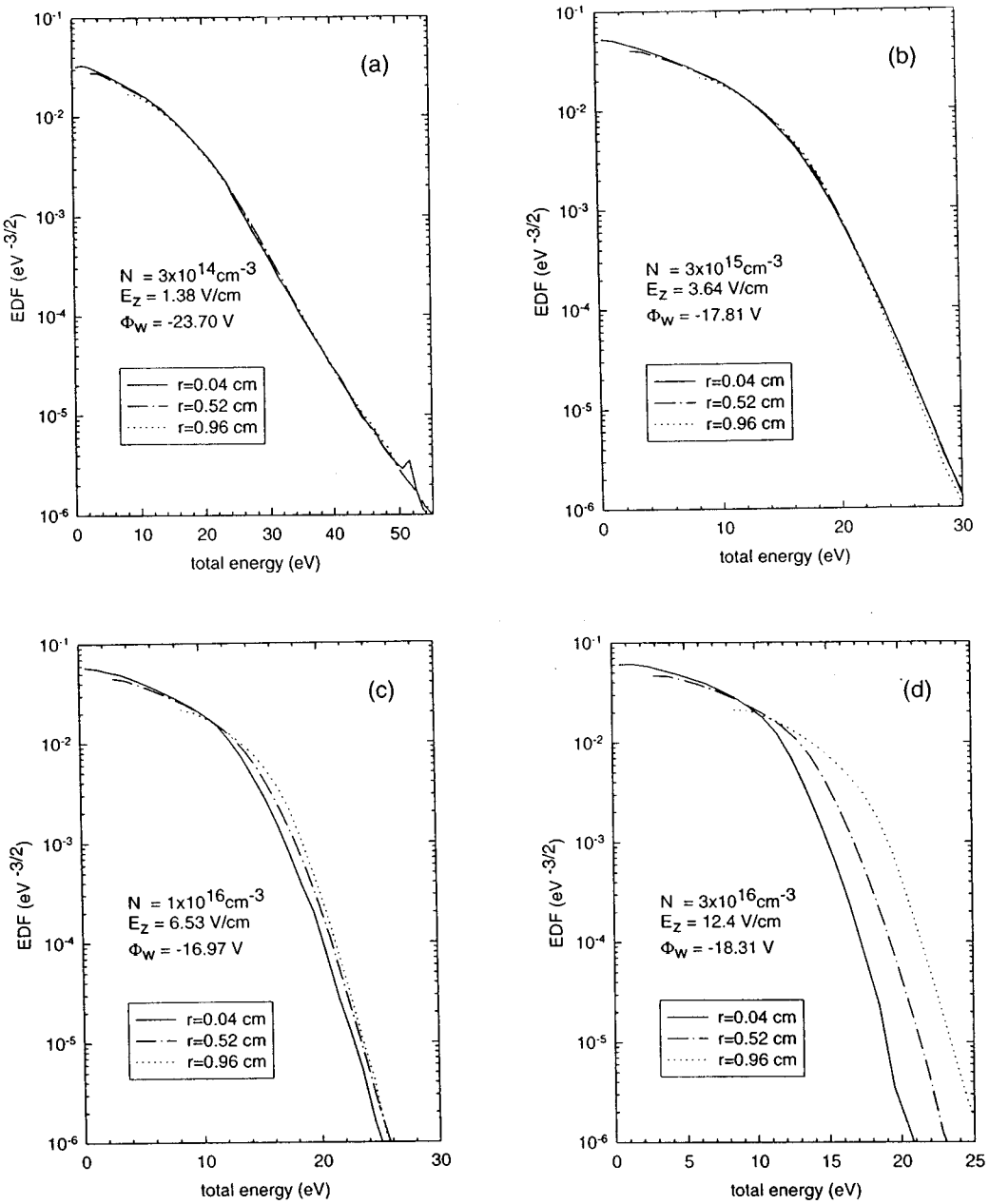

FIG. 2. EDF's from the Monte Carlo calculations at different radial positions plotted as functions of the total energy. The EDF's are normalized to the electron density at $r=0.04$ cm.

removal of the electrons from the high energy tail of the EDF. The results presented in Fig. 1 are consistent with previously obtained results [25,27], in which the wall loss of electrons was not consistently included. It should be noted that even for total energies significantly higher than the potential energy at the wall, the nonlocal behavior of the EDF prevails at the lower neutral gas densities in spite of the wall losses.

In Fig. 2 we present a more quantitative picture of the radial dependence of the EDF. Monte Carlo results for EDF's in the discharge center ($r=0.04$ cm) at about $R/2$, $r=0.52$ cm, and, at the inner boundary of the last cell before the wall, $r=0.96$ cm, are plotted for various gas densities. For neutral gas densities as high as 3×10^{15} cm^{-3} the EDF's as functions of the total energy agree very well. For a neutral gas density of 1×10^{16} cm^{-3} the nonlocal behavior of the EDF begins to break down and it disappears totally for $N=3\times10^{16}$ cm^{-3}. The upper limit for a nonlocal EDF of $N\times R<1\times10^{16}$ cm^{-2} in an argonlike model gas is consistent with results of previous investigations [25,27], and with the intuitive criterion $\lambda_\varepsilon \gtrsim R$ [55]. The wall losses of electrons, which have been neglected in most previous investigations, do not lead to a reduction of the range of applicability for a nonlocal model for the EDF.

In order to investigate the loss cone it is necessary to study the angle-resolved EDF's. In Fig. 3 we present the EDF resolved in the azimuthal angle ϕ and the cosine of the polar angle ϑ referenced to the discharge axis (with $\cos\vartheta=1$ in the direction of the electric field) at $N=3\times10^{15}$ cm^{-3} sampled at three radial positions. The

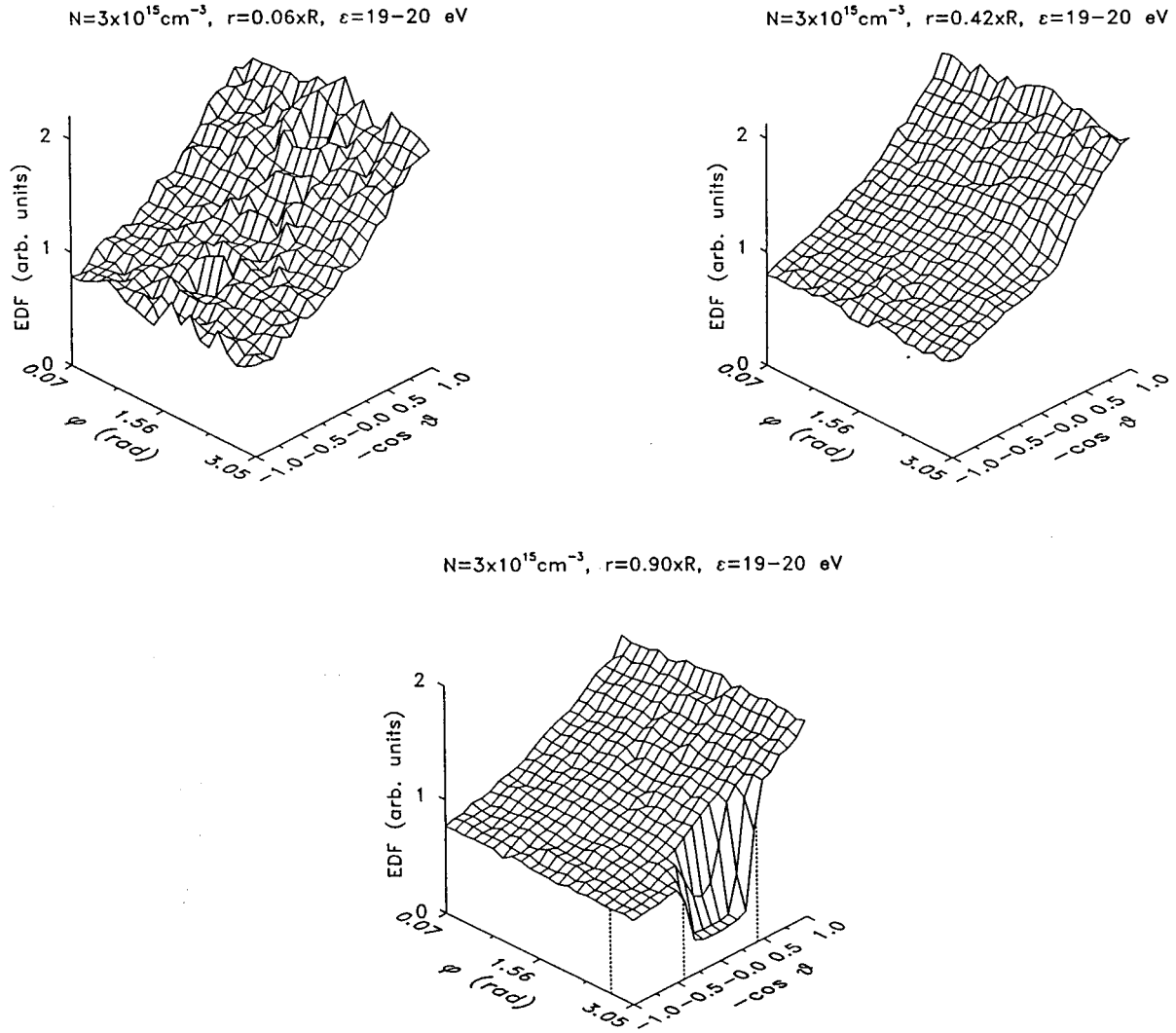

FIG. 3. The EDF resolved in the velocity angle space for $N=3\times10^{15}$ cm^{-3} at different radial positions. The EDF has been sampled in three radial bins and over an energy interval of 1 eV. The dashed lines show the aperture angle found from Eq. (27).

angle $\phi=0$ denotes an electron moving normally toward the nearest wall. For each plot we merged three radial bins in order to improve the statistics, and the center positions of each interval is given in the plots. At this gas density $\lambda_m\approx3$ mm for the energy shown. For the EDF close to the wall the effect of the loss cone is quite visible. It should be noted that the effect of the loss cone is found at $\phi=\pi$. This means that the EDF is not depleted of the electrons flying toward the wall, but of those electrons which have hit the wall but do not return. The EDF is actually depleted in the ''anti-loss-cone.'' The dashed lines show the aperture angle of the loss cone to be expected from Eq. (27). They are in good agreement with the Monte Carlo results. It should be noted that the walls of the loss cone are not vertical, since an averaging over the radius and an energy interval of 1 eV has been performed. At $r=R/2\approx2\lambda_m$ the loss cone has almost completely disappeared due to scattering of electrons into the loss cone. It is totally invisible in the center of the discharge. It should be noted that the EDF also exhibits a significant anisotropy outside the loss cone region due to the axial electric field visible by the increase of the EDF in a direction antiparallel to the electric field. However, the fact that the EDF increases almost linearly with $-\cos\vartheta$ indicates that the two-term approximation is still accurate especially if the loss cone were absent.

In Fig. 4 we present a plot similar to that above, but this time for a value of N that is ten times lower. The mean free path λ_m is about 3 cm, which corresponds to the almost free flight case. The EDF close to the wall now shows a second loss cone at $\phi=0$. This loss cone is the ''anti-loss-cone'' caused by wall losses at the adjacent wall of the discharge tube. Moving toward the center the loss cones show exactly the behavior that was predicted in the discussion of Eq. (40). While its polar aperture angle remains almost constant, it widens in the azimuthal direction. In the center both loss cones merge to form a loss band. The difference between the level of the EDF at the bottom of the loss cone and the EDF at the outside edges of the cone decreases exponentially with the distance from the wall as $\propto\exp((r-R)/\lambda_m)$. The fact that the bottom of the loss cone remains flat and the walls (almost) vertical when the center is approached is a consequence of our assumption of isotropic scattering. Electrons

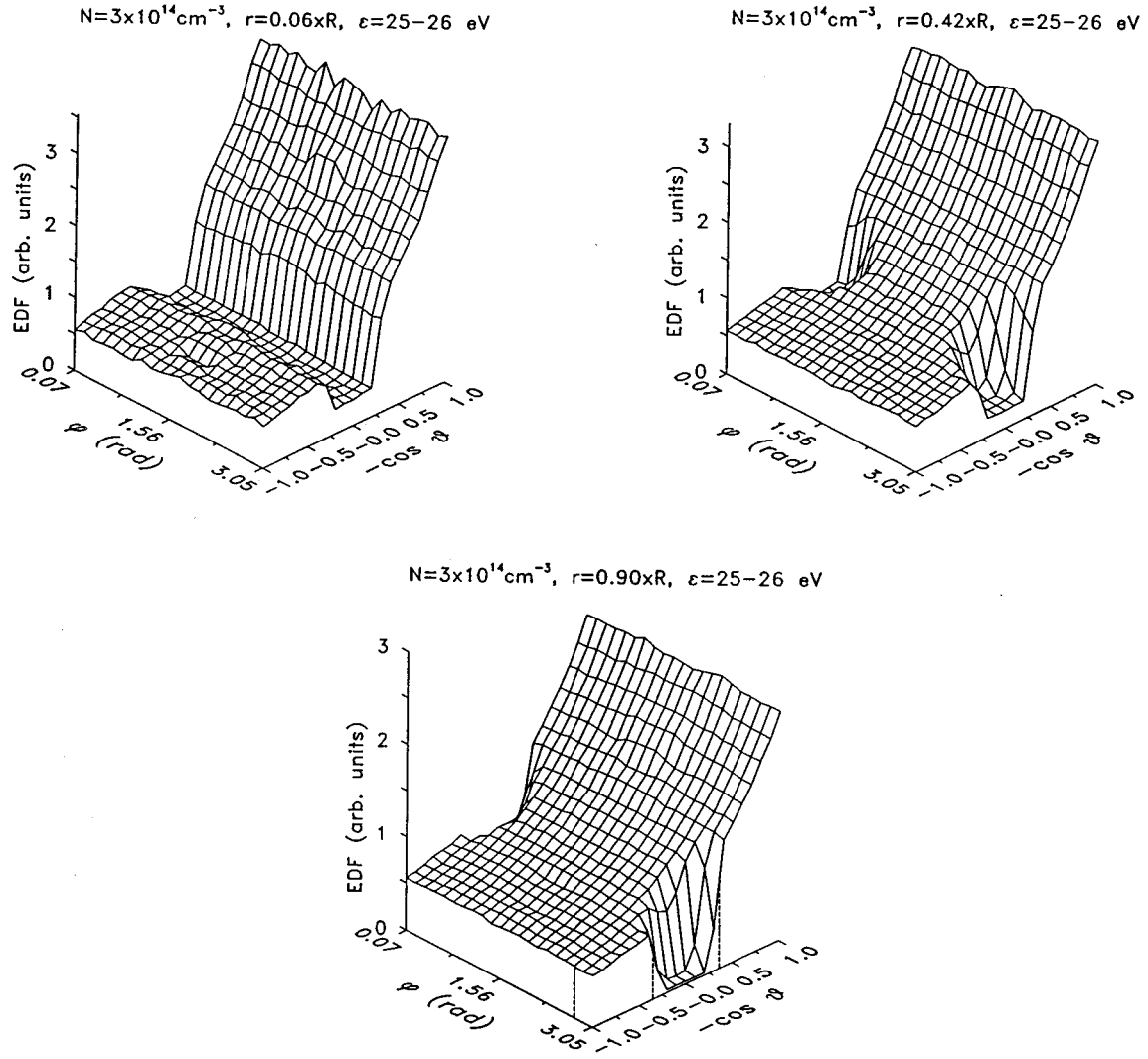

FIG. 4. The EDF resolved in the velocity angle space for $N=3\times10^{14}$ cm^{-3} at different radial positions. The EDF has been sampled in three radial bins and over an energy interval of 1 eV. The dashed lines show the aperture angle found from Eq. (27).

are scattered to every angle within the loss cone with equal probability. Conversely, anisotropic small angle scattering caused, for instance, by Coulomb collisions would lead to a rounded bottom of the cone and smoother walls, since the electrons would diffuse in angle space into the cone. The axial anisotropy of the EDF is even more pronounced than in Fig. 3. The increase of the EDF with $-\cos\vartheta$ is significantly nonlinear. This shows that even in the absence of the loss cone, higher order harmonics in the spherical harmonics expansion would be present, and that the two-term approximation would be questionable. These results should be kept in mind when a comparison with nonlocal calculations are performed, which are formally based on the two-term approximation.

Figure 5 demonstrates the dependence of the loss cone on the energy. With an increasing energy difference above the wall potential energy, the loss cone angle increases. The analytically predicted aperture angle of the loss cone from Eq. (27) is again in good agreement with the Monte Carlo results.

The results in Figs. 1 and 2, obtained with a benchmark Monte Carlo method, provide evidence that the nonlocal approximation is founded on the correct physical assumptions and that it should thus be qualitatively valid. In the following, we will discuss the quantitative correctness of the nonlocal approximation. In Fig. 6 we compare different solutions of the kinetic equation (21) of the nonlocal approximation with the results of the Monte Carlo method. All calculations have been performed with the same axial electric field E_z and the same wall potential Φ_w which were obtained from the self-consistent Monte Carlo-based model. Nonlocal calculations have been performed without including the wall losses of electrons, and using the lifetime approximation of Eq. (37) including one or two loss cones in the free flight case. In particular the results for the lowest gas densities in Fig. 6 demonstrate the vital importance of including the wall losses in the nonlocal approximation. The nonlocal calculations without wall losses show overpopulated EDF tails and too high mean energies for all neutral gas densities investigated, since the most important channel for the loss of high energy electrons is neglected. The inclusion of the wall losses using Eq. (37) enables us to achieve much better agreement with the Monte Carlo results if both loss cones are properly included. At the lower gas density, when

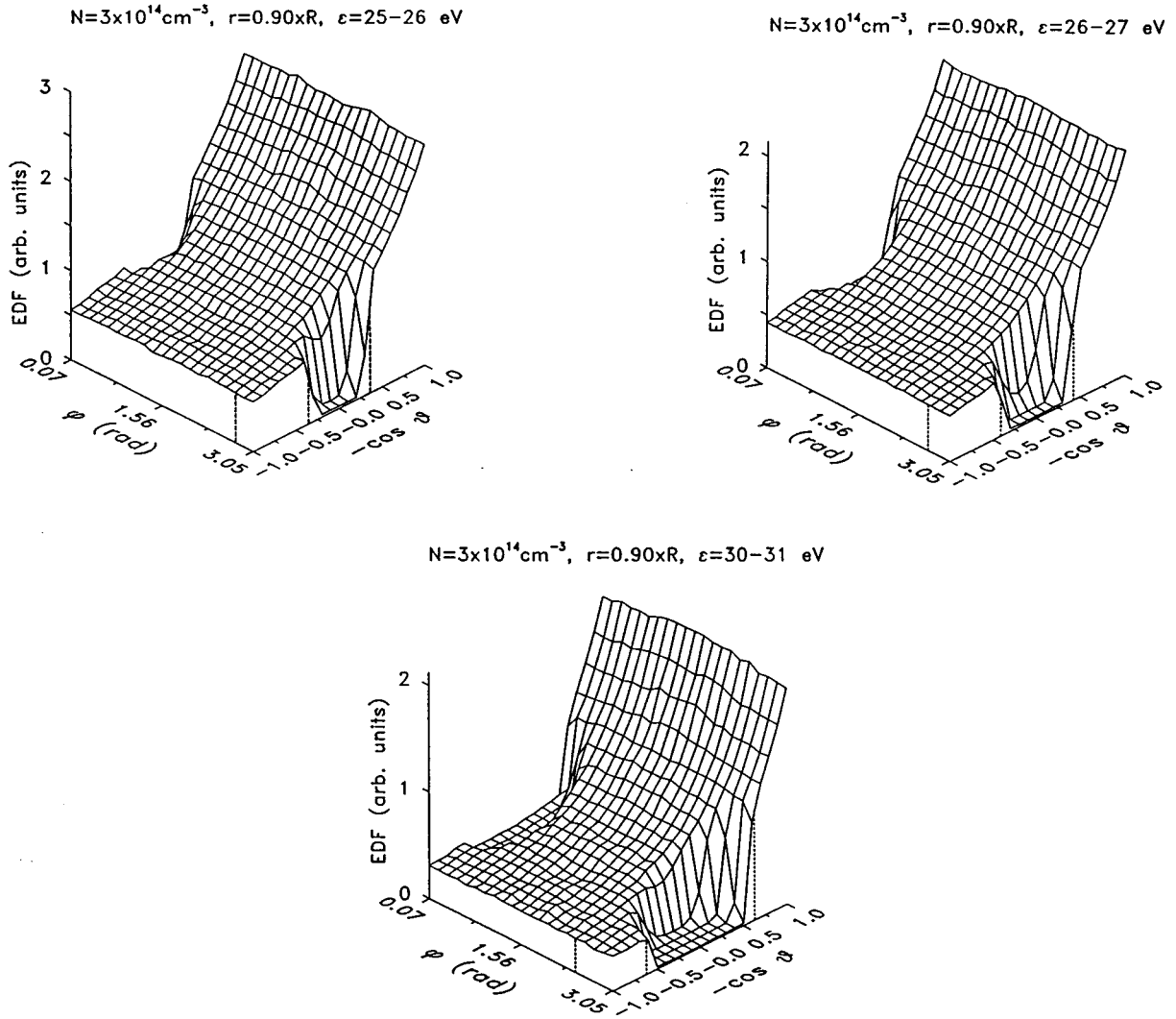

FIG. 5. The EDF resolved in the velocity angle space for $N=3\times10^{14}$ cm^{-3} for different energies above the wall potential. The EDF has been sampled in three radial bins and over an energy interval of 1 eV. The dashed lines show the aperture angle found from Eq. (27).

$\lambda_m \gtrsim R$, the use of only one loss cone yields significantly worse discordance with the Monte Carlo results. Both approximations yield reasonable agreement with the Monte Carlo results at the higher N for the confined and unconfined electrons. It should be noted that for $N=1\times10^{15}$ cm^{-3} the mean free path is already slightly smaller than the discharge radius. The good agreement of the solutions using one and two loss cones in Eq. (37) visible in Figs. 6(c) and 6(d) shows that the wall losses are predominantly determined by the diffusion time of the electrons, τ_{diff}. In general one can state that nonlocal calculations including the wall losses are in very good agreement with the Monte Carlo results for confined electrons. Relatively small deviations occur, usually above the potential energy at the wall due to the approximate description of the unconfined electrons. The slight deviations at very low energies reflect the deviations in the high energy tail of the EDF due to the different particle source terms from ionization. The drastic errors caused by the neglect of the wall losses in the nonlocal calculations, particularly at low neutral gas densities, originate in the fact that the wall loss of electrons, in the energy range where it is possible, has an even stronger effect on the EDF than the ionization collisions. At lower gas densities, ionization represents a larger fraction of the total inelastic processes than at higher pressures. The fraction of ionization processes in the total number of inelastic processes $\overline{n\nu_i}/(\overline{n\nu_i}+\overline{n\nu_{\text{ex}}})$ obtained from the Monte Carlo model is 0.571 for $N=1\times10^{14}$ cm^{-3}, 0.452 for $N=3\times10^{14}$ cm^{-3}, 0.318 for $N=1\times10^{15}$ cm^{-3}, and 0.203 for $N=3\times10^{15}$ cm^{-3}.

At first glance the good agreement of the nonlocal calculations, which are based on the two-term approximation, and the Monte Carlo results may seem surprising, since our Monte Carlo results have demonstrated significant deviations from the two-term approximation at lower neutral gas densities. However, our results prove that in spite of the considerable anisotropy of the EDF, the nonlocal approximation yields quantitatively reasonable results, and is thus still applicable even under these extreme conditions. This is based on the fact that the EDF reflects the fraction of time which an electron spends during its lifetime in the discharge in some energy interval. The simple and physically transparent method of finding the mean lifetime of an electron in the discharge before it escapes to the wall is obviously capable

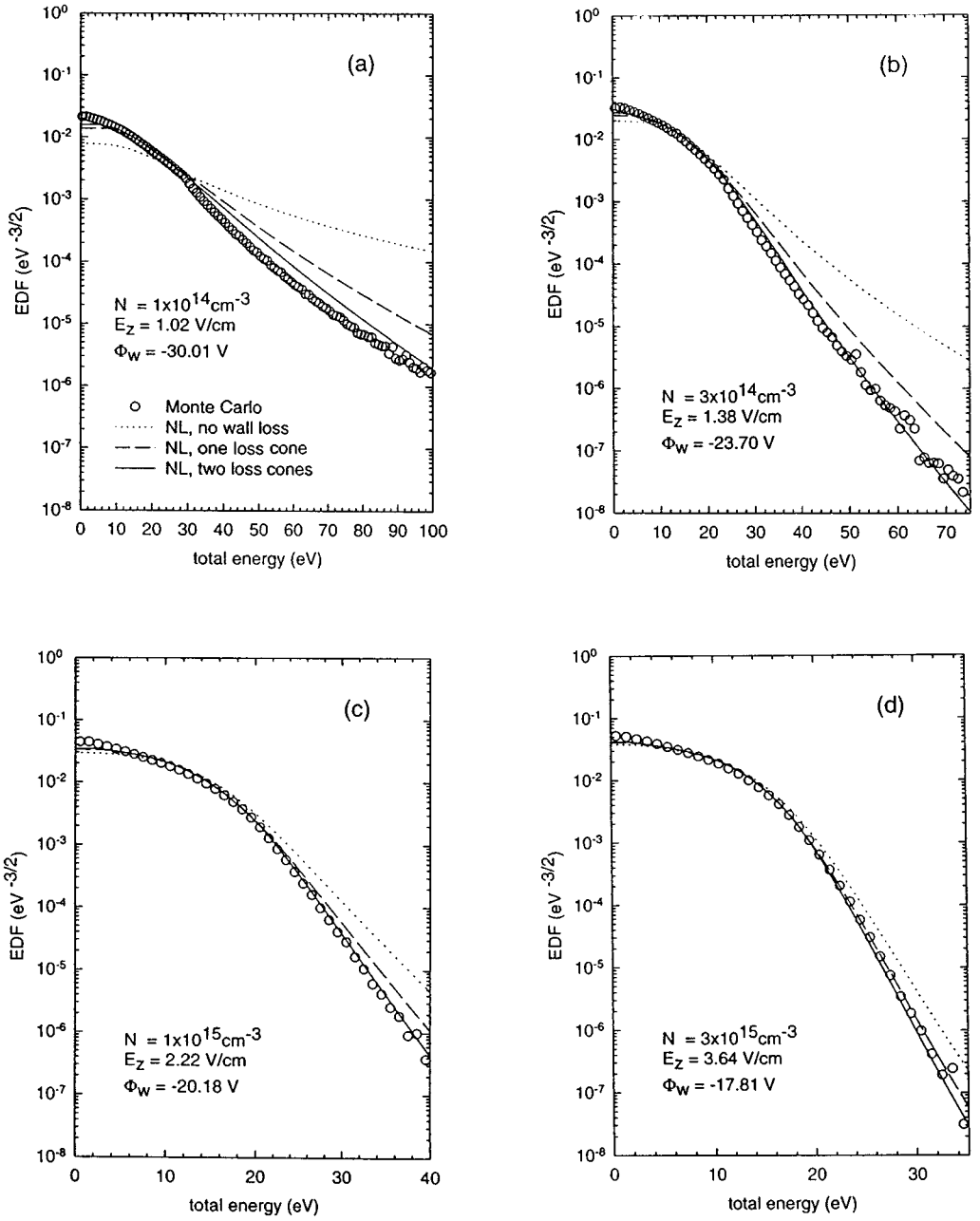

FIG. 6. Comparison of EDF's from the Monte Carlo calculations and from nonlocal calculations with different treatments of the wall losses of the unconfined electrons. All EDF's are evaluated at $r=0.04$ cm with $R=1.0$ cm. The values of the axial electric field E_z and the wall potential Φ_w are the self-consistent values from the Monte Carlo model.

of producing quantitatively reasonable results, even if formal mathematical validity criteria seem to be violated.

In the following we investigate to what extent the differences in the distribution functions affect the macroscopic plasma parameters. In Fig. 7 the self-consistent electric field strengths as obtained from the Monte Carlo model and the nonlocal discharge model with different treatment of the wall losses are depicted. Both nonlocal calculations, which include the wall losses with one or two loss cones, yield a good agreement with the Monte Carlo-based model. Their results are practically indistinguishable. A few percent of the differences shown in Fig. 7 may be due to an imperfect convergence of the Monte Carlo simulations to self-consistent solutions. The maximum deviation from the Monte Carlo results is less than 8% for the neutral gas density below $N=1\times10^{16}$ cm^{-3}, in which the nonlocal approach is valid. However, the nonlocal approach still yields a reasonable value of E_z even at the higher neutral gas density of $N=3\times10^{16}$ cm^{-3}, where the EDF deviates significantly from a nonlocal EDF. This indicates that the EDF obtained from the nonlocal calculations may still represent a reasonable spatial average of the EDF. The nonlocal calculation may thus still yield reasonable spatial averages of the ionization rate, which is decisive for the axial electric field strength. The nonlocal calculations, without including the wall losses, yield significantly lower values of E_z than the Monte Carlo calculations or the nonlocal calculations including wall losses. This behavior corresponds to the higher

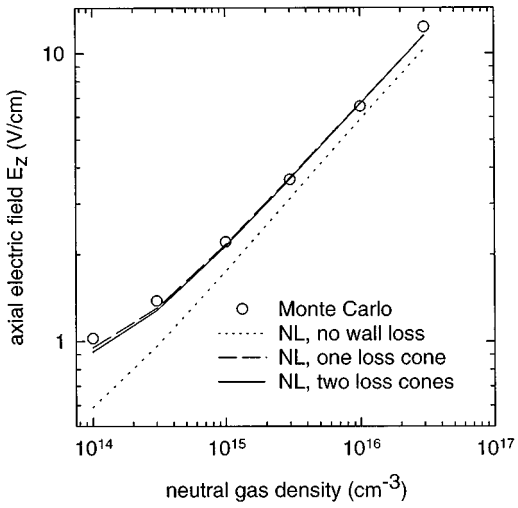

FIG. 7. The self-consistent axial electric fields E_z from the Monte Carlo and nonlocal discharge models with different treatments of the wall losses of the unconfined electrons as a function of the neutral gas density N. The two nonlocal calculations which include wall losses are slightly below the Monte Carlo results, and partially overlap.

population of high energy part of the EDF compared to the other approaches (or reality) (see Fig. 6), which has to be compensated for by lower E_z in order to achieve the particle balance.

The differences between the two approaches using one or two loss cones primarily affect the self-consistent wall potential Φ_w rather than E_z. The self-consistent values of the wall potential from the Monte Carlo model and the two nonlocal calculations including wall losses with one and two loss cones are shown in Fig. 8. The results of the nonlocal model using two loss cones agree with the Monte Carlo results within better than 2.5 V in the applicable range of the nonlocal approximation, $N<1\times10^{16}$ cm^{-3}, except for the lowest neutral gas density. This corresponds to a deviation of

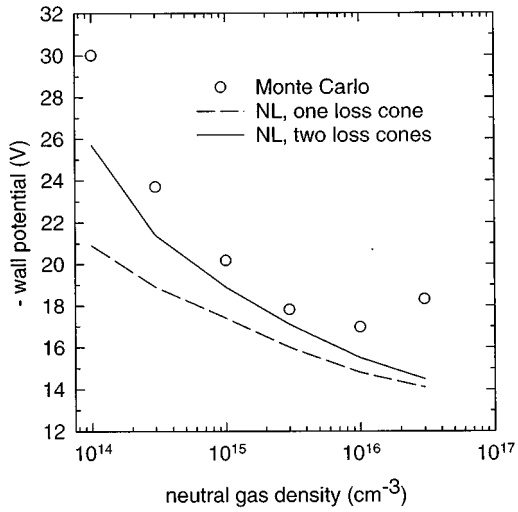

FIG. 8. The self-consistent wall potentials Φ_w from the Monte Carlo and nonlocal models including the wall losses of the unconfined electrons as a function of neutral gas density N.

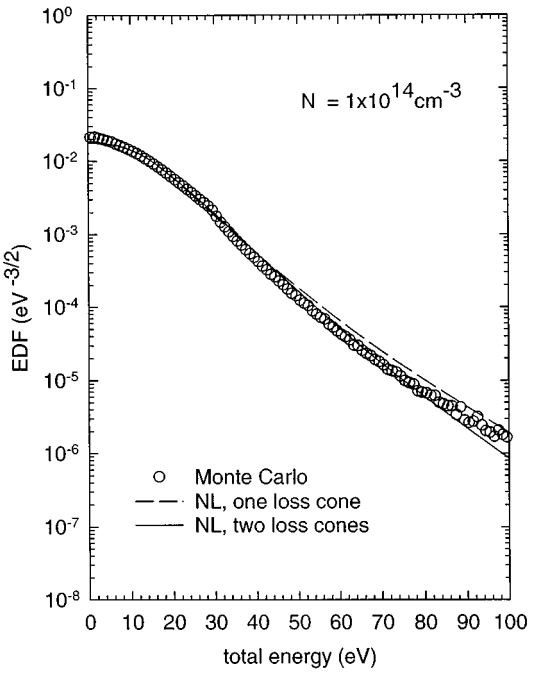

FIG. 9. Comparison of EDF's form the Monte Carlo model and from the nonlocal models including the wall losses of the unconfined electrons each calculated with its self-consistent axial electric field E_z and wall potential Φ_w.

less than 8%, except for the lowest neutral gas density with a deviation of about 15%. In this range of neutral densities the magnitudes of the self-consistent wall potential from the nonlocal calculations using Eq. (37) with two loss cones are consistently lower than the results from the Monte Carlo method, since for the same E_z and Φ_w the nonlocal EDF's showed an excess of high energy electrons as compared to the Monte Carlo results. A decrease of the magnitude of the wall potential increases the amount of wall losses. Hence the nonlocal calculations using Eq. (37) with one loss cone yields consistently smaller $|\Phi_w|$ than the calculations using two cones. Significantly larger deviations for Φ_w appear at $N>3\times10^{16}$ cm^{-3}, where the nonlocal approach is not expected to apply.

It should be noted that the nonlocal EDF's and the Monte Carlo EDF's look almost identical if each calculation uses its own self-consistent E_z and Φ_w. This is demonstrated by Fig. 9 for a neutral gas density of $N=1\times10^{14}$ cm^{-3}. The comparison in Fig. 6(a) at the same $R\times N$ shows larger discordance, because E_z and Φ_w in the nonlocal calculations were fixed at the values from the self-consistent Monte Carlo simulation.

In Fig. 10 we compare the radial profiles of the mean kinetic energy obtained from the Monte Carlo model and the self-consistent nonlocal calculations including wall losses from Eq. (37) using two loss cones. Each model uses its own self-consistent axial electric field E_z and wall potential Φ_w. The nonlocal results shown here are in good agreement with the Monte Carlo results. The mean energies from the nonlocal model are slightly higher than the Monte Carlo results in the center (about 5%) and approach the Monte Carlo results toward the wall. The Monte Carlo results definitely support the basic prediction of the nonlocal model that the

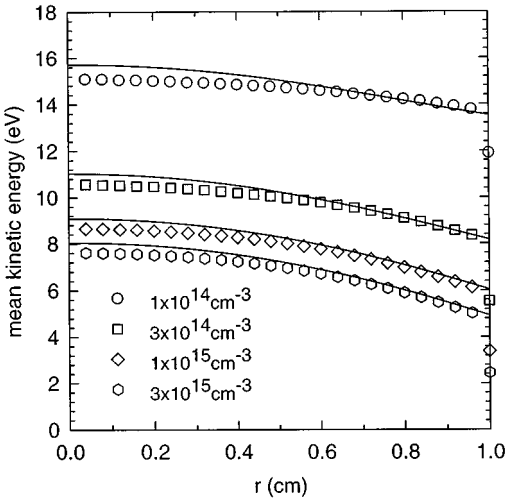

FIG. 10. Comparison of the radial profiles of the mean electron kinetic energy from the Monte Carlo model (symbols) and the nonlocal model with wall losses from Eq. (37) (solid lines). The Monte Carlo and the nonlocal calculation each used its own self-consistent axial electric field E_z and wall potential Φ_w.

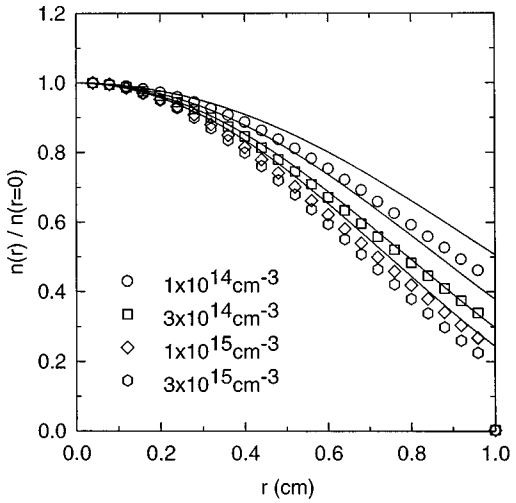

FIG. 11. Comparison of the radial profile of the relative electron density from the Monte Carlo model (symbols) and the nonlocal model with wall losses from Eq. (37) (solid lines). The Monte Carlo and the nonlocal calculation each used its own self-consistent axial electric field E_z and wall potential Φ_w.

mean kinetic energy in a positive column decreases in radial direction if the EDF is convex. This means that the ''local'' temperature of the EDF, $T_e(\varepsilon) = -(d\ \ln(F_0^{(0)})/d\varepsilon)^{-1}$ (i.e., the slope of the EDF in logarithmic presentation) decreases with increasing ε as is the case for our EDF's in the interesting range of energies. Since in the nonlocal model the EDF of kinetic energy is found from the EDF of the total energy by removing the low energy part of the EDF which has a high local temperature, the parts of the EDF with a lower local temperature contribute more strongly to the overall mean kinetic energy and thus lead to the observed decrease of the mean energy toward the wall. The Monte Carlo results show exactly the same behavior. They therefore demonstrate the inaccuracy of the traditional view of the positive column, which assumes that the mean kinetic energy is independent of the radius [57,58].

The self-consistent electron density profiles resulting from the Monte Carlo model and the nonlocal model including wall losses from Eq. (37) with two loss cones are shown in Fig. 11. Each model uses its own self-consistent axial electric field E_z and wall potential Φ_w. Since the different profiles are all normalized to the same central electron density, the deviations between the profiles from the nonlocal and Monte Carlo approaches accumulate at the wall. There one finds deviations of up to 15% with the nonlocal density profiles being slightly higher than their Monte Carlo counterparts. The slower decrease of the electron density just reflects the remaining slight differences in the nonlocal and the Monte Carlo EDF's. As discussed above, these differences seem to be due to the only approximate treatment of the wall losses of the unconfined electrons in the nonlocal approximations.

VI. SUMMARY AND OUTLOOK

In the present investigation we presented an accurate and efficient Monte Carlo method to study the electron kinetics of a positive column plasma. We used this method as a benchmark for testing the nonlocal approximation, which is a very efficient method for modeling the electron kinetics in low-pressure plasmas.

The Monte Carlo results prove that in the low-pressure regime the EDF is nonlocal, i.e., a spatially constant function of total energy. For our argonlike model gas the nonlocal regime for the EDF extends up to a radius times neutral gas density product of $R \times N < 1 \times 10^{16}$ cm^{-2}, which corresponds to a gas pressure of about 0.3 torr at 300 K in a 1-cm-radius positive column. This value is consistent with the more intuitive validity criterion for the nonlocal approximation $\lambda_\varepsilon \gtrsim R$. The nonlocal character of the EDF is not disturbed by the wall losses of electrons.

It has been demonstrated that the wall losses of electrons can be properly included in nonlocal calculations using a simple lifetime approach derived from a wall loss cone. This loss cone or its effect on the EDF has been observed in Monte Carlo simulations. Its scaling and the correctness of the analytic formula describing its aperture angle have been demonstrated. It also has been shown that in the free-flight case two loss cones are present: one loss cone to the nearest wall and one cone to the opposite wall.

The quantitative comparisons conducted between the Monte Carlo based-model and discharge models based on the nonlocal approach demonstrated the importance of including the wall losses of unconfined electrons in the nonlocal approximation. EDF's calculated using the nonlocal model without the wall losses showed significant deviations from the Monte Carlo results for the same E_z and Φ_w. A good agreement between both methods is achieved if the wall losses are included in the nonlocal model. Usually the inclusion of wall losses from Eq. (37) with two loss cones in the free-flight case yields the best agreement of nonlocal calculations with the Monte Carlo results. Within the validity range of the nonlocal approximation agreements within 8% for the axial electric field strengths and the wall potential (except for the lowest neutral gas density considered), within

5% for the mean kinetic energies and 15% for the electron density profiles, were achieved with the nonlocal model including the wall losses from Eq. (37).

In particular, we demonstrated that nonlocal calculations yield good quantitative results, even if a significant anisotropy of the EDF exists at low pressures. In this case the two-term spherical harmonic approximation, which is used in the nonlocal approximation, becomes questionable. However, our results prove that the nonlocal approximation is valid nevertheless, if the physically based lifetime approach is used for describing the wall losses.

From the above results we conclude that the nonlocal approximation produces a very accurate description of the confined electrons and a reasonably accurate description for the unconfined electrons, within its range of validity. The high computational efficiency of nonlocal models is a major advantage in the modeling of low-pressure discharges. In our particular case, computation times of about 1 min for the self-consistent nonlocal calculations were achieved in comparison to calculation times of the order of several hours to several days for the Monte Carlo code when tracking 10^6 electrons.

In the present study we demonstrated the value of an efficient Monte Carlo technique as a benchmark method for testing and improving simpler approximations methods. Further improvements of the Monte Carlo–based positive column model are planned. By implementing a fluid description of the ions, a self-consistent potential profile in the plasma should be obtained. The efficiency of the present Monte Carlo approach can be conserved by approximating the self-consistent potential by a piecewise parabolic function. With this improved model the positive column at higher pressures will be investigated in future studies in order to test the range of validity of the local approximation.

ACKNOWLEDGMENTS

The authors are indebted to Professor Lev D. Tsendin for stimulating discussions and for carefully reading the manuscript. One of the authors (U.K.) was supported by the Alexander von Humboldt foundation. This research was supported by the University of Wisconsin Graduate School, by the General Electric Company, and National Institute of Standards and Technology under the Advanced Technology Program (No. 70NANB3H1373), and by the National Science Foundation under Grant ECS 93-20515.

[1] G. G. Lister, J. Phys. D **25**, 1649 (1992).
[2] M. J. Druyvesteyn, Z. Phys. **64**, 781 (1930).
[3] B. Davydov, Phys. Z. Sowetunion **8**, 59 (1935).
[4] P. M. Morse, W. P. Allis, and E. S. Lamar, Phys. Rev. **48**, 412 (1935).
[5] J. P. Boeuf and E. Marode, J. Phys. D **15**, 2169 (1982).
[6] M. J. Kushner, J. Appl. Phys. **54**, 4958 (1983).
[7] M. J. Kushner, J. Appl. Phys. **61**, 2784 (1987).
[8] P. L. G. Ventzek, T. J. Sommerer, R. J. Hoekstra, and M. J. Kushner, Appl. Phys. Lett. **63**, 605 (1993).
[9] P. L. G. Ventzek, R. J. Hoekstra, and M. J. Kushner, J. Vac. Sci. Technol. B **12**, 461 (1994).
[10] C. K. Birdsall, IEEE Trans. Plasma Sci. **19**, 65 (1991).
[11] M. Surendra, D. B. Graves, and I. J. Morey, Appl. Phys. Lett. **56**, 1022 (1990).
[12] M. Surendra and D. B. Graves, Appl. Phys. Lett. **59**, 2091 (1991).
[13] M. Surendra and D. B. Graves, IEEE Trans. Plasma Sci. **19**, 144 (1991).
[14] V. Vahedi, G. DiPeso, C. K. Birdsall, M. A. Liebermann, and T. D. Rognlien, Plasma Sources Sci. Technol. **2**, 261 (1993).
[15] V. Vahedi, C. K. Birdsall, M. A. Liebermann, G. DiPeso, and T. D. Rognlien, Plasma Sources Sci. Technol. **2**, 273 (1993).
[16] W. N. G. Hitchon, D. J. Koch, and J. B. Adams, J. Comput. Phys. **83**, 79 (1989).
[17] T. J. Sommerer, W. N. G. Hitchon, and J. E. Lawler, Phys. Rev. Lett. **63**, 2361 (1989).
[18] T. J. Sommerer, W. N. G. Hitchon, and J. E. Lawler, Phys. Rev. A **39**, 6356 (1989).
[19] W. N. G. Hitchon, G. J. Parker, and J. E. Lawler, IEEE Trans. Plasma Sci. **21**, 228 (1993).
[20] G. J. Parker, W. N. G. Hitchon, and J. E. Lawler, Phys. Fluids B **5**, 646 (1993).
[21] G. J. Parker, W. N. G. Hitchon, and J. E. Lawler, Phys. Rev. E **50**, 3210 (1994).
[22] V. A. Feoktistov, A. M. Popov, O. B. Popovicheva, A. T. Rakhimov, T. V. Rakhimova, and E. A. Volkova, IEEE Trans. Plasma Sci. **19**, 163 (1991).
[23] P. M. Meijer, W. J. Goedheer, and J. D. P. Passchier, Phys. Rev. A **45**, 1098 (1992).
[24] M. J. Hartig and M. J. Kushner, J. Appl. Phys. **73**, 1080 (1993).
[25] C. Busch and U. Kortshagen, Phys. Rev. E **51**, 280 (1995).
[26] D. Uhrlandt and R. Winkler, J. Phys. D **29**, 115 (1996).
[27] U. Kortshagen, C. Busch, and L. D. Tsendin, Plasma Sources Sci. Technol. **5**, 1 (1996).
[28] U. Kortshagen and L. D. Tsendin, Appl. Phys. Lett. **65**, 1355 (1994).
[29] U. Kortshagen, I. Pukropski, and L. D. Tsendin, Phys. Rev. E **51**, 6063 (1995).
[30] V. Kolobov and W. N. G. Hitchon, Phys. Rev. E **52**, 972 (1995).
[31] I. B. Bernstein and T. Holstein, Phys. Rev. **94**, 1475 (1954).
[32] C. M. Ferreira and J. Loureiro, J. Phys. D **16**, 2471 (1983).
[33] C. M. Ferreira and J. Loureiro, J. Phys. D **17**, 1175 (1984).
[34] E. V. Karoulina and Y. A. Lebedev, J. Phys. D **21**, 411 (1988).
[35] E. V. Karoulina and Y. A. Lebedev, J. Phys. D **25**, 401 (1992).
[36] A. B. Sá, C. M. Ferreira, S. Pasquiers, C. Boisse-Laporte, P. Leprince, and J. Marec, J. Appl. Phys. **70**, 4147 (1991).
[37] P. A. Sá, J. Loureiro, and C. M. Ferreira, J. Phys. D **25**, 960 (1992).
[38] U. Kortshagen, J. Phys. D **26**, 1230 (1993).
[39] V. Kolobov, G. J. Parker, and W. N. G. Hitchon, Phys. Rev. E **53**, 1110 (1996).
[40] K. Wiesemann, Ann. Phys. (Leipzig) **23**, 275 (1969).
[41] V. A. Godyak and R. B. Piejak, Appl. Phys. Lett. **63**, 3137 (1993).

[42] U. Kortshagen, Phys. Rev. E **49**, 4369 (1994).
[43] W. Schottky, Physik. Z **25**, 635 (1924).
[44] L. Tonks and I. Langmuir, Phys. Rev. **34**, 876 (1929).
[45] M. A. Biondi, Phys. Rev. **93**, 1136 (1954).
[46] A. P. Zhilinsky, I. F. Liventseva, and L. D. Tsendin, Zh. Tekh. Fiz. **47**, 304 (1977) [Sov. Phys. Tech. Phys. **22**, 177 (1977)].
[47] J. H. Ingold, in *Gaseous Electronics*, edited by M. N. Hirsh and H. J. Oskam (Academic, New York, 1978).
[48] J. von Neumann, Natl. Bur. Stand. (U.S.) Appl. Math. Ser. **12**, 36 (1951).
[49] H. R. Skullerud, J. Phys. B **2**, 696 (1969).
[50] S. L. Lin and J. N. Bardsley, J. Chem. Phys. **66**, 435 (1977).
[51] L. D. Tsendin, Plasma Sources Sci. Technol. **4**, 200 (1995).
[52] V. I. Kolobov and V. A. Godyak, IEEE Trans. Plasma Sci. **23**, 503 (1995).
[53] I. P. Shkarofsky, T. W. Johnston, and M. P. Bachynski, *The Particle Kinetics of Plasmas* (Addison-Wesley, Reading, MA, 1966).
[54] V. E. Golant, A. P. Zhilinsky, and I. E. Sakharov, *Fundamentals of Plasma Physics* (Wiley, New York, 1980).
[55] L. D. Tsendin, Zh. Eksp. Teor. Fiz. **66**, 1638 (1977) [Sov. Phys. JETP **39**, 805 (1974)].
[56] L. D. Tsendin and Y. B. Golubovskii, Zh. Tekh. Fiz. **47**, 1839 (1977) [Sov. Phys. Tech. Phys. **22**, 1066 (1977)].
[57] R. M. Howe, J. Appl. Phys. **24**, 881 (1953).
[58] W. Verweij, Philips Res. Rep. Suppl. **2**, 62 (1961).